

# Multicolor Coding of Cells with Cationic Peptide Coated Quantum Dots

B. Christoffer Lagerholm,<sup>†,‡</sup> Miaomiao Wang,<sup>§</sup> Lauren A. Ernst,<sup>†</sup> Danith H. Ly,<sup>§</sup> Hongjian Liu,<sup>||</sup> Marcel P. Bruchez,<sup>||</sup> and Alan S. Waggoner<sup>\*,†,‡</sup>

*Molecular Biosensor and Imaging Center, Department of Biological Sciences, and Department of Chemistry, Mellon Institute, Carnegie Mellon University, 4400 Fifth Avenue, Pittsburgh, Pennsylvania USA 15213, and Quantum Dot Corporation, 26118 Research Road, Hayward, California 94545*

Received May 11, 2004; Revised Manuscript Received August 16, 2004

## ABSTRACT

Quantum dots are a new class of fluorophores, whose more prominent characteristics include size-tunable, narrow, fluorescence emission bands and broad overlapping excitation spectra of multiple color dots. Here, we present an efficient, versatile, and gentle approach for intracellular delivery of quantum dots that is easily extended to multicolor optical coding of mammalian cells. In this method, a nine residue biotinylated L-arginine peptide is used to enhance delivery of streptavidin conjugated quantum dots into mammalian cells.

Fluorescence has long been a favored method of detection in a variety of biological applications. Recent advances in fluorescence detection has brought us brighter, more stable and more spectrally distinct dye and protein fluorophores;<sup>1–3</sup> however, limitations including minimal spectral excitation overlap of dyes with distinct emission spectra, broad emission spectra, and susceptibility to photobleaching persist. Quantum dots are a new class of fluorophores which may stand to revolutionize the use of fluorescence in biology. In contrast to conventional fluorophores, quantum dots are excitable over a broad wavelength range stretching from the UV and up to slightly less than their emission peak, have narrow, size-tunable, emission bands, and are resistant to photobleaching.<sup>4,5</sup>

There has been a recent surge in the number of publications on biological applications of quantum dots. These papers have described a variety of in vitro and in vivo applications<sup>6–10</sup> including methods for labeling cells with quantum dots<sup>11–15</sup> either by nonspecific cell surface binding of dihydrolipoic acid coated quantum dots,<sup>12</sup> albumin<sup>14</sup> or Pep-1,<sup>15</sup> or by specific cell surface binding of avidin conjugated quantum dots to biotinylated cell surfaces<sup>12</sup> or by use of transferrin,<sup>11</sup> antibody,<sup>12</sup> or serotonin<sup>13</sup> conjugated quantum dots. These approaches resulted in quantum dot internalization by endocytosis and with no documented

cytotoxic effects.<sup>12,14,15</sup> Quantum dots have also been used for coding microbeads for biological assays.<sup>16</sup> This type of quantum dot multiplexed reagent, which provides a means for coding thousands of biological molecules, is likely to find a use in parallel high-throughput screening of drug candidates. However, a direct method for coding cells by single quantum dots is likely to perturb cell function less than the use of quantum dot coded micron sized beads.

There has been considerable interest in using short arginine-rich peptide sequences for intracellular delivery of a variety of macromolecules.<sup>17</sup> These sequences, which are generally referred to as protein transduction domains (PTDs), include short segments from the human immunodeficiency virus 1 (HIV-1) transcriptional activator Tat protein, the *Drosophila* homeotic transcription protein antennapedia (Antp), and the herpes simplex virus structural protein VP22, as well as homopolymers of arginine.<sup>18</sup> PTDs have so far been used for intracellular delivery of proteins, 40 nm diameter magnetic nanoparticles,<sup>19</sup> and even 200 nm diameter liposomes.<sup>20</sup> Since the diameter of quantum dots (typically between 5 and 15 nm depending on core composition and emission wavelength) falls well within the documented size range of cargoes that have been internalized by PTDs, we reasoned that this approach should also work for delivering quantum dots intracellularly.

In this work, we evaluated the use of two versions of a nine residue biotinylated L-arginine (L-Arg<sub>9</sub>) peptide, one of which had an additional six-carbon linker between the biotin moiety and the C-terminus of the peptide (biotin-C<sub>6</sub>-(L-Arg)<sub>9</sub>), for intracellular delivery of quantum dots. We found that coupling either of the biotin-(L-Arg)<sub>9</sub> peptides to quantum

\* Corresponding author. E-mail: waggoner@andrew.cmu.edu.

<sup>†</sup> Molecular Biosensor and Imaging Center.

<sup>‡</sup> Department of Biological Sciences.

<sup>§</sup> Department of Chemistry.

<sup>||</sup> Quantum Dot Corporation.

<sup>‡</sup> Current address: Department of Cell and Developmental Biology, University of North Carolina at Chapel Hill, CB# 7090, Chapel Hill, North Carolina 27599.

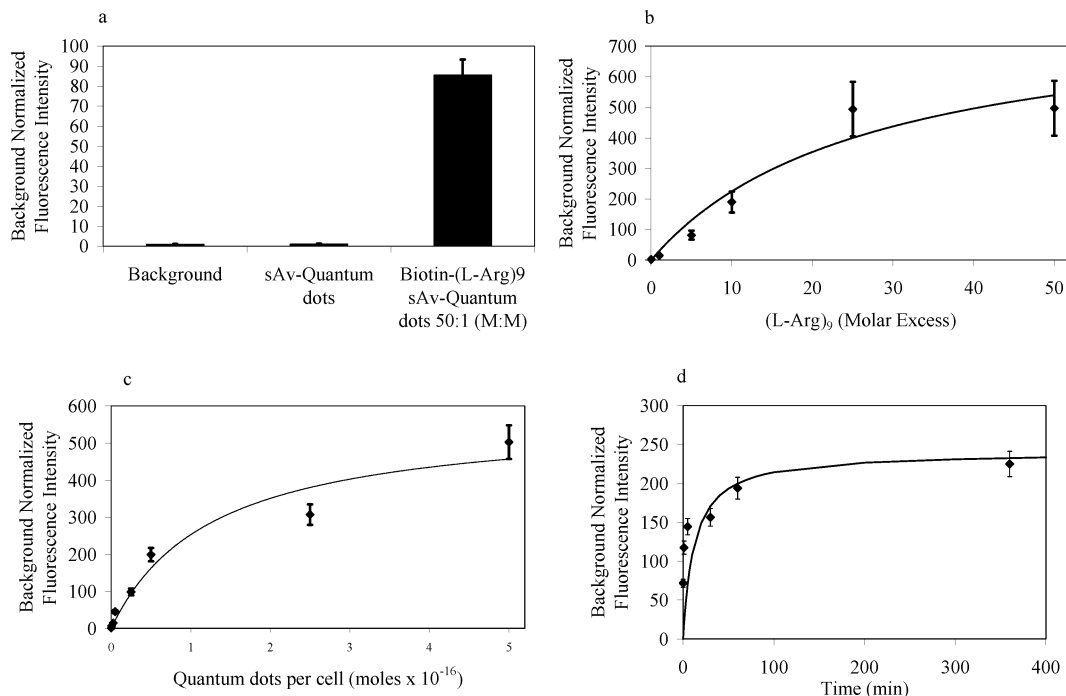


**Figure 1.** (a–d) Flow cytometric analysis of quantum dot uptake characteristics in Swiss 3T3 mouse fibroblasts. Values shown are the geometric mean fluorescence intensities normalized by the cellular autofluorescence  $\pm$  standard deviations. In (b–d), values,  $F$ , were fit to a saturable binding model,  $F = F_{\max}x/(K + x)$ , where the parameter  $K$  is the value of the dependent variable at half saturation. (a) The cell uptake efficiency of quantum dots ( $1.25 \times 10^{-17}$  mol/cell) precomplexed by a 50-fold molar excess of biotinylated (L-arginine)<sub>9</sub> is greater by almost 2 orders magnitude as compared to incubation with bare quantum dots. In contrast, the fluorescence intensity of cells incubated with quantum dots alone is no different from that of cellular autofluorescence. (b) Half-saturation of quantum dot uptake was reached at 27-fold molar excess of biotinylated (L-Arg)<sub>9</sub> peptide ( $5 \times 10^{-18}$  moles quantum dots per cell; 30 min), (c) after incubation with  $1.3 \times 10^{-16}$  moles quantum dots per cell (50-fold molar excess biotinylated (L-Arg)<sub>9</sub> peptide; 30 min), and (d) at incubation times of 12 min ( $2.5 \times 10^{-17}$  moles quantum dots per cell; 50-fold molar excess biotinylated (L-Arg)<sub>9</sub> peptide).

dots via streptavidin–biotin linkages resulted in an increase of roughly 2 orders of magnitude in intracellular uptake of quantum dots in a variety of mammalian cell types (embryonic mouse fibroblasts (Swiss 3T3), human endothelial cells (HeLa), and human osteoblast-like cells (MG63)) as determined by flow cytometry and fluorescence microscopy (Figure 1a). We confirmed that quantum dots were internalized by use of transmission electron microscopy, which showed that quantum dots were concentrated in intracellular vesicles characteristic of endosomes and lysosomes (Supporting Information, Figure 1).

A similar increase in uptake efficiency was seen using core–shell quantum dots that were directly coated with cationic surfactants di-dodecyl (C<sub>12</sub>) or di-hexadecyl (C<sub>16</sub>) di-methylammonium bromide as compared to quantum dots coated with lecithin, suggesting that the highly cationic nature of the peptide and not its composition may be responsible for the increased uptake. Because we observed rapid quantum dot precipitation upon formation of the biotin-C<sub>6</sub>-(L-Arg)<sub>9</sub>–sAv quantum dot complex, we only continued experiments with the linkerless biotin-(L-Arg)<sub>9</sub> peptide. Henceforth, all the data presented are from use of the (L-Arg)<sub>9</sub> peptide which had the biotin moiety attached straight to the C-terminal end of the peptide.

The cellular uptake characteristics of the biotin-(L-Arg)<sub>9</sub>–sAv quantum dot complex were studied in detail in Swiss 3T3 mouse fibroblasts and with quantum dots with an

emission maxima at 655 nanometers (sAv-655 quantum dots). We found that cells are readily labeled while adherent to a substrate or in suspension. However, labeling of adherent cells typically leads to significant binding of the biotin-(L-Arg)<sub>9</sub>–sAv quantum dot complex to the extracellular matrix, leading to a decrease in the amount of quantum dots taken up by the cells. Optimum labeling was obtained by incubating freshly trypsinized cells with the precomplexed biotin-(L-Arg)<sub>9</sub>–sAv quantum dots, in suspension (0.5 mL total volume) at 4 °C, while mixing for at least 30 min, followed by incubation at 37 °C. We also found that cells are readily labeled in tissue culture media containing 10% calf serum, indicating that the cell surface affinity for the biotin-(L-Arg)<sub>9</sub>–sAv quantum dot complex is significant. We determined that the cellular uptake reaches half saturation at about 25-fold molar excess of peptide (Figure 1b) after incubation with about  $1 \times 10^{-16}$  moles of quantum dots per cell (Figure 1c), and after about 10 minutes of incubation (Figure 1d).

We next determined if the biotin-(L-Arg)<sub>9</sub> peptide could also be used to code cells with combinations of multiple color quantum dots. To demonstrate quantum dot optical coding feasibility, we used quantum dots that had minimal emission spectral overlap (emission maxima of 565 (fwhm 32 nm), 605 (fwhm 23 nm), and 655 nanometers (fwhm 30 nm); sAv-565, sAv-605, and sAv-655 quantum dots) and a binary intensity scheme (0 or 1) for a total of 2<sup>3</sup> optical coding possibilities. Quantum dot cell coding was then done by

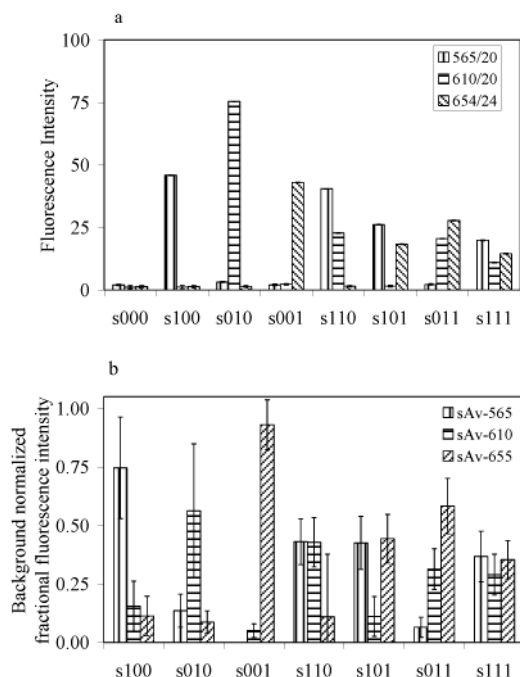


**Figure 2.** Quantitative analysis of cell multicolor coding with quantum dots. Swiss 3T3 fibroblasts were labeled with (s000) blank control, (s100) sAv-565 quantum dots, (s010) sAv-605 quantum dots, (s001) sAv-655 quantum dots, (s110) sAv-565 and sAv-605 quantum dots, (s101) sAv-565 and sAv-655 quantum dots, (s011) sAv-605 and sAv-655 quantum dots, and (s111) sAv-565, sAv-605, and sAv-655 quantum dots. (a) Analysis by flow cytometry. Values shown are the geometric mean of the fluorescence intensity of labeled cells divided by the fluorescence intensity of unlabeled cells  $\pm$  standard deviations from two separate experiments for each color channel. (b) Analysis by fluorescence microscopy. Values shown are the mean fractional fluorescence intensities  $\pm$  standard deviations for two to four cells for each coding scenario.

separately incubating cells, as before, with one of eight possible combinations of quantum dots (50 molar excess biotin-(L-Arg));  $2.5 \times 10^{-18}$  moles total quantum dots/cell). However, to compensate for differences in emission intensity of the quantum dots, for multicolor labeling we used four molar equivalences of sAv-565 quantum dots to one molar equivalent of sAv-605 quantum dots to two molar equivalences of sAv-655 quantum dots. As a result, the fluorescence intensity in each color channel was at a maximum for single color labeled cells but the integrated fluorescence intensity for all channels was approximately constant, as was presumably the amount of internalized quantum dots.

Following cell uptake, the quantum dot codes were read quantitatively by measuring the fluorescence intensities in each of three appropriately chosen detector color channels on a cell-to-cell basis by flow cytometry (Figure 2a) or at the subcellular level (pixel-to-pixel) by fluorescence microscopy (Figure 2b) or qualitatively by fluorescence microscopy (Figure 3) (see Methods). In the case of detection by flow cytometry, each code was detected at a minimum background normalized fluorescence intensity of about 10 (i.e., for intensities of “1” of all three colors in the same cell, s111; sAv-565:  $9.9 \pm 1.3$ , sAv-605:  $9.8 \pm 5.7$ , and sAv-655:  $10.4 \pm 3.1$ ) (Figure 2a). Analysis of the same scenario by fluorescence microscopy, yielded background subtracted,

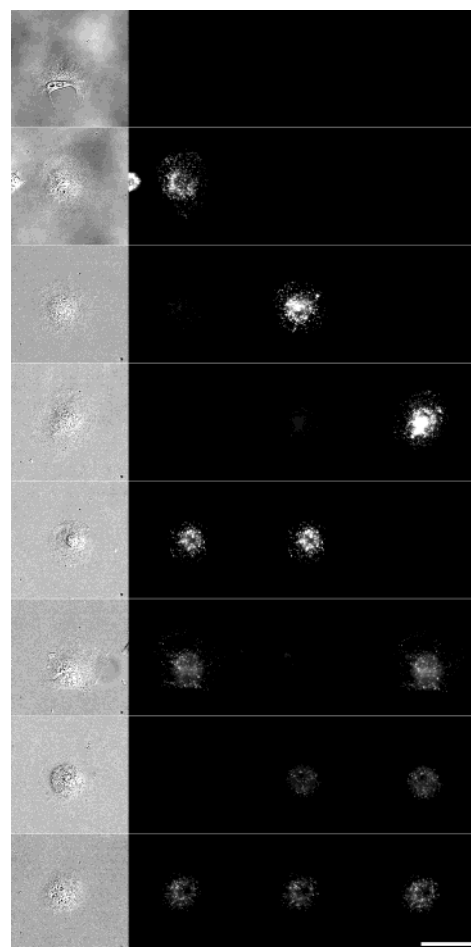


**Figure 3.** Qualitative analysis of cell multicolor coding by fluorescence microscopy. Swiss 3T3 fibroblasts were labeled in suspension as described. Images shown are (column 1) differential interference contrast (DIC), (column 2) fluorescence with 565/20 nm emission filter, (column 3) fluorescence with 610/20 nm emission filter, and (column 4) fluorescence with 654/24 nm emission filter. Cells were labeled with (row 1) blank control (row 2) sAv-565 quantum dots, (row 3) sAv-605 quantum dots, (row 4) sAv-655 quantum dots, (row 5) sAv-565 and sAv-605 quantum dots, (row 6) sAv-565 and sAv-655 quantum dots, (row 7) sAv-605 and sAv-655 quantum dots, (row 8) sAv-565, sAv-605, and sAv-655 quantum dots. Fluorescence images within each column were scaled to the same brightness and contrast values such that the fluorescence signal overlap of each color quantum dots into adjacent detector channels was minimized (scale bar = 20  $\mu$ m).

mean fractional fluorescence intensities per pixel of sAv-565:  $0.37 \pm 0.11$ , sAv-605:  $0.29 \pm 0.09$ , and sAv-655:  $0.35 \pm 0.08$  (Figure 2b) where the background subtracted, mean fractional fluorescence intensity was calculated only for pixels with a fluorescence intensity greater than the mean plus 10 standard deviations of the background intensity in that channel. We could also read the codes qualitatively using fluorescence microscopy by finding brightness and contrast values of images within each color channel that excluded cellular autofluorescence while not saturating images with actual quantum dot fluorescence signal and by then displaying the whole set of images with those values (Figure 3). Hence, this method of coding cells with multiple colors of quantum dots resulted not only in readily detectable, uniform labeling at the cell-to-cell level as determined by flow

cytometry but also at the subcellular level (pixel-to-pixel) as determined by fluorescence microscopy. Despite the precautions taken to minimize fluorescence signal overlap, there are instances where fluorescence signal from one color quantum dots is detected in an adjacent channel. While this does not prevent the detection of the optical codes as described, it will limit the number of additional usable codes. It is possible to further minimize overlap either by selecting quantum dots whose emission spectra is further separated or possibly by selecting fluorescence band-pass filters with a narrower bandwidth.

The endocytic localization of the biotin-(L-Arg)<sub>9</sub>-sAv quantum dot complex in our case is consistent with recent reports on the mechanism of transduction of PTD linked cargo.<sup>21,22</sup> While the endocytic quantum dot localization limits the usefulness of this method for determining cell proliferation since endosomes/lysosomes are not evenly divided during mitosis,<sup>23</sup> it could also be a potential advantage since the quantum dots, once internalized, are concentrated yet isolated from most cell signaling events. In addition, it is still possible to determine cell lineage from the fluorescence intensity in each color channel, especially by fluorescence microscopy where even single quantum dot containing endosomes/lysosomes are readily detectable. This is in particular true since optical coding with the biotin-(L-Arg)<sub>9</sub>-sAv quantum dot complex extends to the subcellular level. We have in separate work shown that quantum dots are stable in endosomes/lysosomes in phagocytic cells in liver, spleen, and lymph nodes in living mice for at least 4.5 months.<sup>24</sup> It is then possible that the biotin-(L-Arg)<sub>9</sub>-sAv quantum dot method for coding cells as described could be used to track cells in vivo over very long time periods. The described method for coding cells could also be used for cell tracking experiments in vitro, especially in cases involving co-culturing of multiple cell types or multiple genetically engineered cell lines.

In this paper, we describe a very efficient, versatile, and gentle (i.e., efficient labeling in 10% calf serum) method for coding mammalian cells with quantum dots. In the current format there are eight optical codes (three colors and two intensities) that are easily detected by appropriately chosen color channels in either flow cytometry or fluorescence microscopy. The method can also easily be extended to more optical codes by use of additional spectrally separated quantum dots. It is also possible that the total number of distinct optical codes may be increased by use of more than two intensities. The use of additional codes, however, will be limited by spectral overlap of different colored quantum dots. Another advantage of this method is that it relies on now commercially available streptavidin-coated quantum dots (Quantum Dot Corporation; Haywood, CA) and an easily obtainable custom synthesized nine residue (L-Arg)<sub>9</sub> peptide and is therefore readily adapted for use in any experimental setting.

**Acknowledgment.** We thank Drs. Byron Ballou and Greg Fisher for helpful comments and Joseph P. Suhon for expert technical assistance in electron microscopy. This work was supported by NIH grant number R01 EB 000364.

**Supporting Information Available:** Experimental methods and transmission electron microscopy image of internalized quantum dots. This information is available free of charge via the Internet at <http://pubs.acs.org>.

## References

- (1) Mujumdar, R. B.; Ernst, L. A.; Mujumdar, S. R.; Lewis, C. J.; Waggoner A. S. *Bioconjugate Chem.* **1993**, *4*, 105–111.
- (2) Zhang, J.; Campbell, R. E.; Ting, A. Y.; Tsien, R. Y. *Nat. Rev. Mol. Cell Biol.* **2002**, *3*, 906–918.
- (3) Panchuk-Voloshina, N.; Haugland R. P.; Bishop-Stewart, J.; Bhalgat, M. K.; Millard, P. J.; Mao, F.; Leung, W. Y.; Haugland, R. P. *J. Histochem. Cytochem.* **1999**, *47*, 1179–1188.
- (4) Watson A.; Wu X.; Bruchez M. *Biotechniques* **2003**, *34*, 296–303.
- (5) Chan, W. C. W.; Maxwell, D. J.; Gao, X.; Bailey, R. E.; Han, M.; Nie, S. *Curr. Opin. Biotechnol.* **2002**, *13*, 40–46.
- (6) Bruchez, M.; Moronne, M.; Gin, P.; Weiss, S.; Alivisatos, A. P. *Science* **1998**, *281*, 2013–2016.
- (7) Larson, D. R.; Zipfel, W. R.; Williams, R. M.; Clark, S. W.; Bruchez, M. P.; Wise, F. W.; Webb, W. W. *Science* **2003**, *300*, 1434–1436.
- (8) Wu, X.; Liu, H.; Liu, J.; Haley, K. N.; Treadway, J. A.; Larson, J. P.; Ge, N.; Peale, F.; Bruchez, M. P. *Nat. Biotechnol.* **2003**, *21*, 41–46.
- (9) Dubertret, B.; Skourides, P.; Norris, D. J.; Noireaux, V.; Brivanlou, A. H.; Libchaber, A. *Science* **2002**, *298*, 1759–1762.
- (10) Åkerman, M. E.; Chan, W. C. W.; Laakkonen, P.; Bhatia S. N.; Ruoslahti, E. *Proc. Natl. Acad. Sci. U.S.A.* **2002**, *99*, 12617–12621.
- (11) Chan, W. C. W.; Nie, S. *Science* **1998**, *281*, 2016–2018.
- (12) Jaiswal, J. K.; Mattoussi, H.; Mauro, J. M.; Simon, S. M. *Nat. Biotechnol.* **2003**, *21*, 47–51.
- (13) Rosenthal, S. J.; Tomlinson, I.; Adkins, E. M.; Schroeter, S.; Adams, S.; Swafford, L.; McBride, J.; Wang, Y.; DeFelice, L. J.; Blakely, R. D. *J. Am. Chem. Soc.* **2002**, *124*, 4586–4594.
- (14) Hanaki, K.; Momo, A.; Oku, T.; Komoto, A.; Maenosono, S.; Yamaguchi, Y.; Yamamoto, K. *Biochem. Biophys. Res. Commun.* **2003**, *302*, 496–501.
- (15) Mattheakis, L. C.; Dias, J. M.; Choi, Y. J.; Gong, J.; Bruchez, M. P.; Liu, J.; Wang, E. *Anal. Biochem.* **2004**, *327*, 200–208.
- (16) Han, M.; Gao, X.; Su, J. Z.; Nie, S. *Nat. Biotechnol.* **2001**, *19*, 631–635.
- (17) Wadia, J. S.; Dowdy, S. F. *Curr. Opin. Biotechnol.* **2002**, *13*, 52–56.
- (18) Wender, P. A.; Mitchell, D. J.; Pattabiraman, K.; Pelkey, E. T.; Steinman, L.; Rothbard, J. B. *Proc. Natl. Acad. Sci. U.S.A.* **2000**, *97*, 13003–13008.
- (19) Lewin, M.; Carlesso, N.; Tung, C. H.; Tang, X. W.; Cory, D.; Scadden, D. T.; Weissleder, R. *Nat. Biotechnol.* **2000**, *18*, 410–414.
- (20) Torchilin, V. P.; Rammohan, R.; Weissig, V.; Levchenko, T. S. *Proc. Natl. Acad. Sci. U.S.A.* **2001**, *98*, 8786–8791.
- (21) Richard, J. P.; Melikov, K.; Vives, E.; Ramos, C.; Verbeure, B.; Gait, M. J.; Chernomordik, L. V.; Lebleu, B. *J. Biol. Chem.* **2003**, *278*, 585–590.
- (22) Wadia, J. S.; Stan, R. V.; Dowdy, S. F. *Nat. Med.* **2004**, *10*, 310–315.
- (23) Bergeland, T.; Widerberg, J.; Bakke, O.; Nordeng, T. W. *Curr. Biol.* **2001**, *11*, 644–651.
- (24) Ballou, B.; Lagerholm, B. C.; Ernst, L. A.; Bruchez, M. P.; Waggoner, A. S. *Bioconjugate Chem.* **2004**, *15*, 79–86.

NL049295V